

www.acsami.org Research Article

Solid Electrolytes for Li-S Batteries: Solid Solutions of Poly(ethylene oxide) with Li_xPON- and Li_xSiPON-Based Polymers

Eleni Temeche, Xinyu Zhang, and Richard M. Laine*



Cite This: ACS Appl. Mater. Interfaces 2020, 12, 30353-30364



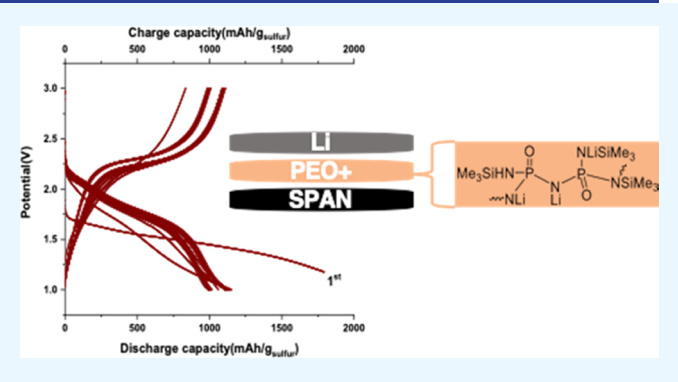
ACCESS

Metrics & More

Article Recommendations

s Supporting Information

ABSTRACT: We report here efforts to synthesize free-standing, dry polymer electrolytes that exhibit superior ionic conductivities at ambient for Li–S batteries. Co-dissolution of poly(ethylene oxide) (PEO) ($M_{\rm n}$ 900k) with Li_xPON and Li_xSiPON polymer systems at a ratio of approximately 3:2 followed by casting provides transparent, solid-solution films 25–50 μ m thick, lowering PEO crystallinity, and providing measured impedance values of 0.1–2.8 × 10⁻³ S/cm at ambient. These values are much higher than simple PEO/Li⁺ salt systems. These solid-solution polymer electrolytes (PEs) are (1) thermally stable to 100 °C; (2) offer activation energies of 0.2–0.5 eV; (3) suppress dendrite formation; and (4) enable the use of lithium anodes at current densities as high as 3.5 mAh/cm². Galvanostatic cycling of SPAN/PEs/Li cell (SPAN =



sulfurized, carbonized polyacrylonitrile) shows discharge capacities of 1000 mAh/ g_{sulfur} at 0.25C and 800 mAh/ g_{sulfur} at 1C with high coulumbic efficiency over 100 cycles.

KEYWORDS: LiPON, PEO, polymer precursors, polymer electrolyte, lithium-sulfur battery

1. INTRODUCTION

The potential benefits from all-solid-state batteries (ASSBs) have generated intense academic and commercial efforts to replace liquid electrolytes with solid electrolyte materials that avoid the flammability of current liquids, protect against dendrite growth leading to short circuiting, and offer higher energy densities by allowing the use of metallic lithium as an anode with a theoretical capacity of 3860 mAh/g.^{1–3}

The search for solid electrolytes can be divided into polymeric and glass/ceramic with the former having the potential to be easily introduced commercially because it represents "drop-in" technology in that polymeric materials as separators are already widely extant in state-of-the-art liquid electrolyte batteries. 4 Glass/ceramic electrolytes offer potential advantages being stable at temperature extremes and wide electrochemical stability windows not accessible to polymers. However, glass/ceramic electrolytes normally require much higher processing temperatures and their introduction to the assembly of ASSBs would entail introducing large-scale changes to battery assembly processes. 5,6 Polymer electrolytes offer several advantages compared to glass/ceramic electrolytes, such as enhanced resistance to volume variations during cycling, excellent flexible geometries, and as noted just above, processability.7,

Although polymer electrolytes have demonstrated multiple advantages since their discovery in 1973,⁹ little progress has been made in commercializing them. Dry solid polymer

electrolytes such as poly(ethylene oxide) (PEO)–LiX [X:Tf⁻, SO₄²⁻, ClO₄⁻, BF₄⁻, SbF₆⁻ and PF₆⁻] systems offer poor Li⁺ conductivities of 10⁻⁵–10⁻⁶ S/cm at room temperature, representing a significant barrier to practical applications. ^{10,11} PEO–LiX systems have been the subject of multiple studies because the ethyleneoxy monomer units easily coordinate Li⁺ ions via a crown-ether-like mechanism. ¹¹ These coordination complexes can rigidly bind Li⁺ to the point where diffusion is limited primarily because of the ease of crystallization of PEO systems, even when highly cross-linked. ¹² In general, Li⁺ transport (diffusion) occurs preferentially through the amorphous regions of PEO. ^{13,14} This process likely occurs via segmental reorientation of neighboring chains coincident with Li⁺ diffusion. ^{15–17}

However, an alternate explanation to the segmental motion mechanism and the requirement for an amorphous phase in PEO to achieve high ionic conductivities was recently presented in a study that shows that in crystalline PEO–LiX [X: PF₆, AsF₆, SbF₆], Li $^{+}$ ions diffuse through the cylindrical tunnels without the efficacy of segmental motion. ^{18,19} Perhaps

Received: April 3, 2020 Accepted: June 10, 2020 Published: June 10, 2020





both mechanisms are operative, but it is clear that more work must be done. 19

In particular, significant attempts to enhance the room-temperature ionic conductivities of PEO-based electrolytes are reported in many studies through the use of plasticizers, addition of second-phase solids that interfere with crystal-lization, and the choice or concentration of Li⁺ salt.^{20,21} A primary problem with adding organic second phases (plasticizer) is the deterioration of the mechanical properties at the expense of conductivity and some additives are relatively reactive with lithium metal, ^{22,23} narrowing the electrochemical stability window.

The second approach, introducing an inorganic second phase or filler, has also been explored in some detail with inert and active Li⁺ conducting fillers. $^{24-26}$ Inactive fillers improve Li⁺ conductivity by reducing PEO crystallization. Active fillers contribute to Li⁺ conductivity by both reducing PEO crystallinity and by promoting surface Li⁺ transport at PEO/nanofiller interfaces. 27 In previous work, we explored the use of NASICON-type Li⁺ ion conducting nanopowders [Li_{1.3}Al_{0.3}Ti_{1.7}(PO₄)₃] (LATP) in PEO-LiClO₄ systems to realize superior composite electrolytes that exhibit room-temperature ionic conductivities of 10^{-4} S/cm. However, LATP suffers from poor chemical stability due to irreversible reduction of Ti⁴⁺ when in contact with metallic Li. 29

Lithium phosphorous oxynitride (LiPON) has been widely studied since its discovery in the early 90's owing to its negligible electrical conductivity $(10^{-7} \, \mu \text{S/cm})$, ³⁰ high critical current density (>10 mA/cm²), ³¹ wide electrochemical stability window (0–5 V νs Li⁺/Li), ³¹ and high Li⁺ transference number. ³² However, LiPON exhibits poor ionic conductivity (10^{-6} S/cm) at ambient, ³³ restricting its application to microbatteries with limited energy densities and capacities (0.1–5 mAh). ³⁴

LiPON- and PEO-based electrolytes are recommended interlayer materials because of their compatibility when in direct contact with Li-based anodes. Some studies demonstrated the performance of the bilayer structures comprised of LiPON/[Li_{1.5}Al_{0.5}Ge_{1.5}(PO₄)]. The composite structure benefits from these two layers of electrolytes. Specifically, LiPON is a desirable interlayer material owing to its high shear modulus (31 GPa) approximately nine times that of Li metal, suggesting that it can suppress Li dendrite penetration of electrolytes. LiPON thin films are typically deposited onto the ceramic electrolyte by the radio frequency magnetron sputtering technique. LiPON thin films are typically deposited onto the ceramic electrolyte by the radio frequency magnetron sputtering technique. However, gas-phase deposition methods require expensive steps to regulate the coating uniformity, deposition atmospheres, rates, and film thickness. Hence, these methods are challenging for assembling ASSBs for large-scale applications.

Recently, we have demonstrated the design and synthesis of inorganic polymers/oligomers of Li_xPON-, Li_xSiPON-, and Li_xSiPHN-like electrolytes by a low-temperature, low-cost, and solution-processable route. ^{38,39} The development of these polymer electrolytes offers desirable properties superior to LiPON glasses. ³⁸ These polymer electrolytes also offer high Li⁺ transference numbers $(t_{\text{Li}}^+$ 0.7–0.9). ³⁸ Dry solid polymer electrolytes are well-known bi-ionic conductors with t_{Li}^+ < 0.5. ¹¹ The decrease in t_{Li}^+ is ascribed to the fast migration of anions within the polymer matrix, which results in concentration polarization. Electropolarization results in decreases in the overall electrochemical performance of the electrolyte

attributed to increases in internal resistance, voltage drops, and dendritic growth. 41

To minimize polarization and increase $t_{\rm Li}$, the mobility of anions has to be reduced either by anchoring the anions to the polymer backbone or by adding a chelator that selectively traps the anions. To the best of our knowledge, no one has sought to apply LiPON-derived polymer electrolytes as the active filler in PEO systems to achieve single-ion conduction. This provides the motivation to synthesize $\text{Li}_x\text{PON/PEO}$ composite solid electrolytes that profit from these polymer mixtures.

In our efforts to develop Li, PON-, Li, SiPON-, and Li_xSiPHN-like polymer precursors,³⁹ we realized that it might also be possible to use our precursors as the active fillers in PEO systems either as miscible or immiscible but active second phases. Note that because our polymers on heating turn into ceramics, these systems are anticipated to offer flame retardance or resistance unlike most liquid or polymer electrolytes. Below we present a systematic study on the role of Li⁺-ion concentration in PEO/precursor composites on cation-transport properties. The PEO solid-solution films exhibit enhanced ionic conductivities of $\sim 0.1-2 \times 10^{-3}$ S/cm at ambient and low activation energies (0.2-0.5 eV) for cation transport. In addition, galvanostatic cycling of the SPAN/PEs/ Li battery shows discharge capacities of 1000 mAh/g_{sulfur} at 0.25C and 800 mAh/g_{sulfur} at 1C with high (\sim 100%) coulombic efficiency over extensive cycles.

2. EXPERIMENTAL SECTION

2.1. Polymer Synthesis. 2.1.1. Materials. Poly(ethylene oxide) [PEO 4 M and 900k] and Li metal foil (99.9%) were purchased from Sigma-Aldrich (Milwaukee, WI). Acetonitrile (ACN) and tetrahydrofuran (THF) were purchased from Fischer Scientific (Pittsburgh, PA). All raw materials are regent grade.

Using precursor design principles reported elsewhere, $^{43-46}$ we synthesized three Li_xPON-like precursors. The first synthesis method employs oligomeric OP(NH₂)₃, which, following lithiation, produces the Li_xPON precursor, as shown in Scheme S1. A second precursor incorporates Si components based on literature reports that introduction of Si can give rise to fast Li⁺ ion conduction in LiPON, as shown in Scheme S2, $^{47-49}$ providing motivation for this selection. A third precursor was synthesized from chlorophosphazene [Cl₂P = N]₃ and eliminates all oxygen but also incorporates Si and C. Detailed structural compositions and analysis of the polymer precursors can be found elsewhere.

2.2. Synthesis of the PEO/Polymer Precursor Solid-Solution Films. After some trial and error, it was determined that solid solutions of all of the precursors form readily at 60 wt % PEO. Such compositions also gave good-to-excellent conductivities. Table 1 lists the formulation of such 60 wt % PEO/40 wt % polymer precursor solid solutions. PEO ($M_{\rm w}=900{\rm k}$) powder was first dissolved with 18 mL of ACN. The polymer precursor as a THF solution (6 mL) was mixed with the PEO solution and stirred magnetically for 12 h. The obtained clear solution was then cast onto a Teflon plate. After slow solvent evaporation at ambient over 24 h, the resulting transparent

Table 1. List of PEO and Polymer Electrolytes Dissolved in 18 mL of ACN

polymer electrolyte	mass of PEO (g)	mass of polymer electrolyte (g)
Li ₃ PON	0.6	0.21
Li ₆ PON	0.6	0.14
Li ₂ SiPHN	0.9	0.6
Li ₃ SiPON	0.9	0.6
Li ₆ SiPON	0.9	0.6

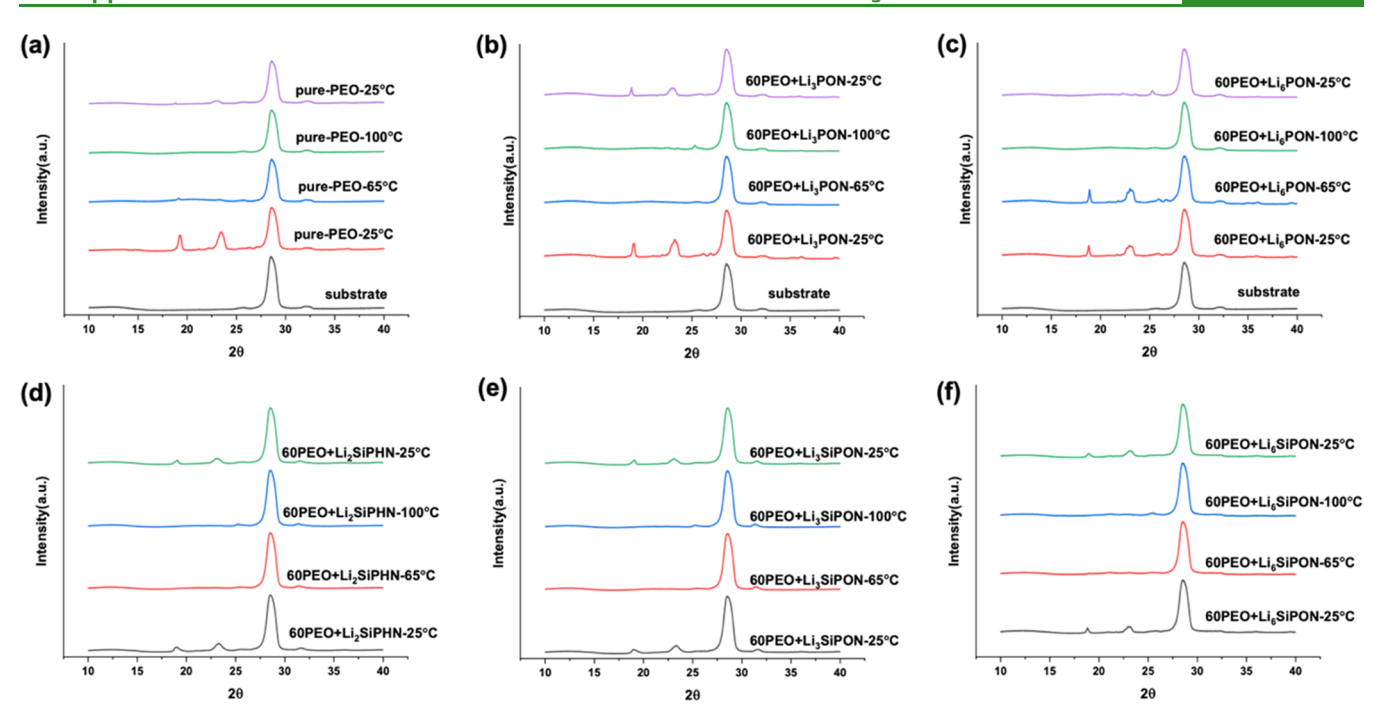


Figure 1. In situ XRD patterns of (a) pure PEO, (b) 60PEO/Li₃PON, (c) 60PEO/Li₆PON, (d) 60PEO/Li₂SiPHN, (e) 60PEO/Li₆SiPON, and (f) 60PEO/Li₆SiPON at selected temperatures.

films were then dried at 3×10^{-3} Torr for 24 h at 65 °C. The dried films are referred to as polymer electrolytes (PEs). Higher PEO concentrations result in poorer ionic conductivity, while lower PEO concentrations result in poorer mechanical properties.

2.3. Symmetric Cell Assembly. Symmetric Li/PE/Li cells were assembled in a glovebox under Ar. Before cell assembly, metallic Li foil (16 mm diameter) was scraped to expose a clean surface. The symmetric coin cells were cycled at ambient using a potentiostat/galvanostat (BioLogic SP300). The critical current densities of the cells were tested using a DC steady-state method in which a constant current (±0.15–7.5 mA) was used.³⁹

Symmetrical cells using (Li/60 wt % PEO + polymer electrolytes/Li) were monitored via chronoamperometry at (direct voltage) DV = 10 mV until a steady-state current was reached. The transference numbers ($t_{\rm Li'}$) of the polymer electrolytes were calculated based on the procedure discussed elsewhere. The cyclic voltammetry (CV) data for the polymer electrolytes was acquired in the potential range of -1 to 6 V vs Li/Li⁺ at a sweep rate of 5 mV/s. The CV measurement was performed in a coin 2032 cell using stainless steel (SS) as the working electrode and Li as the counter and reference electrodes.

2.3.1. Half-Cell Assembly. Half-cells were assembled using SPAN as the cathode, PEs as an electrolyte, and Li metal as the anode. Before cell assembly, the metallic Li (16 mm W X 750 μ m T) was scraped to expose a clean surface. The coin 2032 cells were compressed using a ~0.1 kpsi uniaxial pressure. The electrochemical characterization of the coin cells was performed using a potentiostat/galvanostat (BioLogic SP300). A 10 μ L solution of polymer precursors {(Li₃PON (0.05 g/mL), Li₆PON (0.05 g/mL), Li₂SiPHN (0.08 g/mL), Li₃SiPON (0.1 g/mL), and Li₆SiPON (0.1 g/mL)} dissolved in THF was used in assembling the half-cell to minimize the interfacial impedance between the electrodes and the PEs.

Besides, the cathode and the polymer electrolyte were warm-pressed at 5 kpsi/40 $^{\circ}$ C/2 min to minimize the IR drop caused by the poor interface. The half-cells were then briefly warmed to 60 $^{\circ}$ C in the glovebox to further improve Li/PE contact and to prevent hot spots. The cathode slurry was prepared by mixing SPAN (70 wt %), C65 (15 wt %), and PVDF (15 wt %) in 1-methyl pyrrolidin-2-one. The slurry was then coated on the carbon-coated Al foil. The electrode was heated to 60 $^{\circ}$ C/12 h/vacuum before half-cell assembly.

3. RESULTS AND DISCUSSION

3.1. Characterization of the PEO/Polymer Precursor Solid-Solution Films. Following optimization of the solid-solution systems, we then explored the formulation of PEO/precursor solid-solution composite systems and characterized them by Fourier transform infrared (FTIR), X-ray diffraction (XRD), X-ray photoelectron spectroscopy (XPS), scanning electron microscopy (SEM), differential scanning calorimetry (DSC), and electrochemical impedance spectroscopy (EIS). Detailed analyses of the PEs in symmetric and half-cells are also presented using Li metal and SPAN electrodes.

The FTIRs of the films (Figure S1) heated to 65 °C/24 h/Vac show a peak near 3300–3500, ascribed to ν N–H/O–H. There is a small ν C–H peak ≈ 2900 cm⁻¹. The minor peak around 1400 cm⁻¹ is typical for N–H bending. Besides, peaks at 1090, 1142, and 839 cm⁻¹ correlate to PEO.²⁸

3.1.1. In Situ XRD and XPS Studies of PEs. Rigaku (Rigaku Denki., Ltd., Tokyo, Japan) was used to analyze the crystal structures of the PEs films, as well as pure PEO. Films were heated from 25 to 65° and 100 °C/min at 3 °C/min. The films were then cooled to room temperature. Temperature-dependent in situ XRD was examined with Cu K α radiation of wavelength λ = 1.541 Å operating at 40 kV and 44 mA with high D/teX Ultra 250 detectors in the 10–40° 2 θ range using a step width of 0.02°. The slow scan rate was used to minimize the signal–noise ratio. Graphite was used as a substrate for thermal conductivity and as an internal standard for quantifying peak shifts.

In Figure 1a, the XRD patterns of pure PEO show a large intensity peak at 23.5° 2θ , followed by a second maximum peak at 19.3° , and a doublet peak at 26.45° 2θ corresponding to (112), (120), and (222) planes (PDF: 00-049-2201), respectively.

Table S1 lists the *d*-spacing and peaks for the various PE films at selected temperatures. The peak near 29° 2θ is

ascribed to the graphite substrate. All peak positions shift with respect to the graphite substrate as standard.

Figure 1b-f shows in situ XRD patterns for PEs films. The composite films show the largest intensity peak at 23.3° 2θ , following a second less intense peak at 19° 2θ , and a small peak $\sim 26.2^{\circ}$ 2 θ . The X-ray spectra of the PE films at room temperature exhibit peak shifts toward lower diffraction angles compared to pure PEO, as listed in Table S1. For example, the (112) peak shifts from 19.3° to 18.8° 2θ when Li₆SiPON precursor is introduced. The d-spacings between (112) planes increase from 4.55 to 4.72 Å, suggesting strong interactions with the precursor. Shifts in the XRD peaks can be caused by strain or stress. 50 The differences in crystallization kinetics are attributed to the variation in miscibility between PEO and the precursor systems. Addition of the PEs especially with Me₃Si moieties reduces the crystallinity considerably as demonstrated by broadening and reduction of PEO peak intensities vs graphite.

In Figure 2, the XPS survey provides the elemental compositions of the PE films showing the expected elements

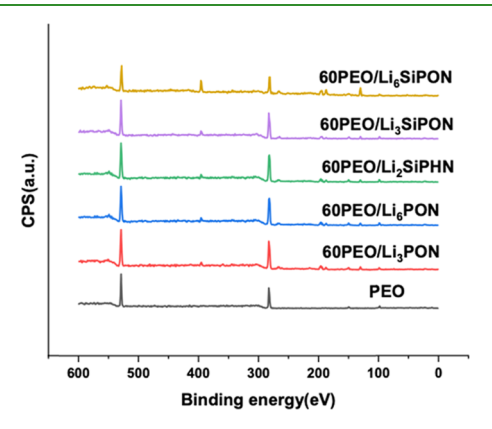


Figure 2. XPS Spectrum (600-0 eV) of PEs and the PEO film.

for Li_xPON and Li_xSiPON with an additional peak for C from PEO. Tables 2 and S2 summarize the obtained XPS results.

Table 2. Calculated Atomic Compositions for the PE Composite Films

ratio	Li ₃ PON	Li ₆ PON	Li ₂ SiPHN	Li ₃ SiPON	Li ₆ SiPON
N/P	1.1	1.1	1.5	1.2	1.0
Li/N	1.9	2.5	1.1	0.9	1.3

The resulting atomic percentage (atom %) demonstrates that the Li/N ratio increases from \sim 0.9 to 1.3 with increasing amounts of LiNH₂ for the 60PEO/Li_xSiPON films. However, this ratio is smaller when compared to the Li₃PON (1.9) and Li₆PON (2.5) polymer composite films. This might be attributed to the introduction of silicon in the polymer precursor. The N/P ratio deduced from the XPS analysis (Table 2) is smaller than what is experimentally calculated (3); this decrease is likely associated with the loss of nitrogen by polymerization. However, compared to gas-phase-deposited Li_xPON materials, the obtained N/P ratios (1–1.5) for the PE films are higher. The relation between the N/P ratio and ionic conductivity is discussed below in Section 3.1.3.

The element bonding environments can be obtained from the XPS analysis. The binding energy of the carbon in all of the polymer composite films coincides with the most intense PEO carbon peak of the $-CH_2-CH_2-O-$ repeat unit.

3.1.2. Microstructure and DSC Studies of PEs. The literature reports that for PEO/Li salt mixtures, the introduction of excess salt reduces the crystallinity and crystallization temperature of the PEO system as a result of cation and ether oxygen interaction. 44 Our PE films do not contain any salt, and thus, the cation and ether oxygen interaction is proposed to occur as a result of cation dissociation from the polymer precursor backbone. The PEO crystallization is directly influenced by the cation dissociation and its interaction with ether oxygens or indirectly governed by the microstructure of the film during crystallization.

Figure 3b-f shows SEMs of the PE films heated to 65 °C/ 24 h/Vac. The film microstructures look very dense. The observed microstructure depends on the preparation procedure, which is critical in optimizing the dispersion of the polymer precursors in the PEO matrix. The 60PEO/Li_xSiPON films' surface morphology appears to be uniform, dense, and smooth. The morphology of the 60PEO/Li₂SiPHN film showed irregular surface with crystalline domains. The introduction of the Li₃PON precursor into the polymer matrix resulted in a spherulitic structure. The diameter of spherulites seems to increase with the increase of Li content (i.e., Li₃PON to Li₆PON), which might be ascribed to the increase in the nucleating center during film formation.⁵² Figure S2 presents the elemental distribution of the polymer electrolytes. Energydispersive X-ray (EDX) map of the Li_xPON and Li_xSiPON films shows well-dispersed signature elements (P, O, N, and C) and (Si, P, O, N, and C), respectively.

To analyze the influence of the polymer precursors on the crystallinity of PEO, we first determined the PEO crystallinity for each PE film using DSC (χ_c). The percent crystallinity was calculated using $\chi_c = \Delta H_{\rm m}/({\rm wt_{PEO}})\Delta H_{\rm m}^0$, where $\Delta H_{\rm m}$ is the melting enthalpy acquired from the DSC measurement and $\Delta H_{\rm m}^0$ is the melting enthalpy of pure crystalline PEO. Literature values for $\Delta H_{\rm m}^0$ range from 188 to 216 J/g. S0,53,54 As such, we assumed that the $\Delta H_{\rm m}^0$ = 206 J/g. S3

Figure 4 shows the DSC thermogram of a pure PEO film and all of the PE films. For the pristine PEO sample, an endotherm is seen at \sim 71 °C for the 1st cycle, which shifts to 69 °C after the 2nd and 3rd cycles. This is ascribed to the melting of crystalline PEO. Pure PEO also exhibits a crystallization exotherm peak near \sim 38 °C. The peak crystallization temperatures ($T_{\rm c}$) can also be determined from the cooling response. The addition of the PEs to PEO decreases $T_{\rm c}$ slightly.

In Figure 4, endotherms are observed for all PE films. Table 3 lists the calculated percent crystallinity and found the melting temperature of these solid-solution electrolyte films. The degree of crystallinity is of the order Li₂SiPHN > Li₆PON > Li₃PON > Li₆SiPON > Li₃SiPON. $T_{\rm m}$ decreases with the introduction of the PEs, suggesting that PEO crystallization is hindered. The crystallization temperature is also reduced from 40 to 38–30 °C, comparing pristine PEO vs the PEs. These results are in good agreement with the XRD peak broadining (Figure 1) and smooth surface microstrcuture observed by SEM micrographs (Figure 3).

3.1.3. Conductivity Studies of PEs. The ionic conductivity is highly correlated with the charge density and mobility of the active spices.⁵⁵ The key design parameters to enhance the ionic conductivity of the polymer precursor electrolyte are three-fold. (1) Decrease the crystallinity of the PEO matrix,⁵⁶ (2)

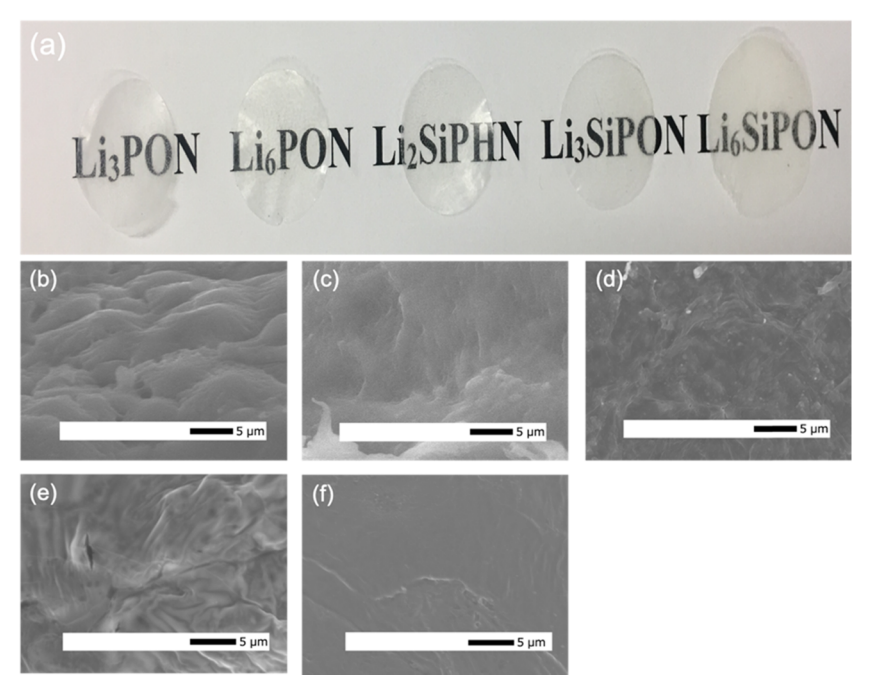


Figure 3. (a) Optical images of PEs and SEM images of (b) 60PEO/Li₃PON, (c) 60PEO/Li₆PON, (d) 60PEO/Li₂SiPHN, (e) 60PEO/Li₃SiPON, and (f) 60PEO/Li₆SiPON heated to 65 °C/24 h/Vac.

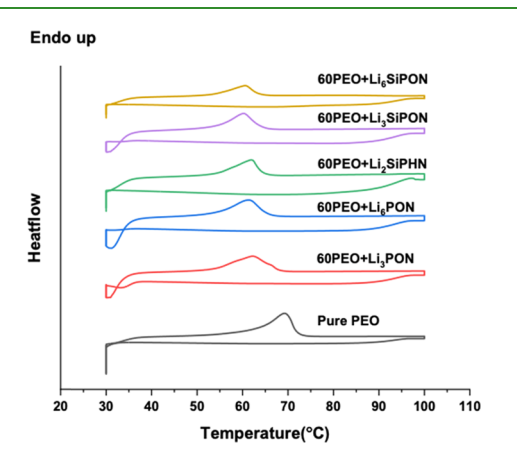


Figure 4. DSC thermograms of pristine PEO and PE films after the 3rd cycle.

Table 3. Thermal Properties of the PEO-Derived Polymer Electrolyte Films

sample	$T_{\rm m}$ (°C)	heat of melting (J/g)	degree of crystallinity (χ_c)
PEO	69	191	93
60PEO/Li ₃ PON	62	93	45
60PEO/Li ₆ PON	62	96	47
60PEO/Li ₂ SiPHN	61	116	56
60PEO/Li ₃ SiPON	58	30	15
60PEO/Li ₆ SiPON	61	60	30

increase the charge carrier densities by increasing the Li⁺ concentration (i.e., Li₃PON to Li₆PON). This is challenging to attain using gas-phase-deposited Li_xPON as Li concentration is almost constant regardless of the deposition method (i.e., rf power).⁵⁷ In addition, dispersing ceramic Li_xPON in the PEO matrix is very difficult. However, our polymer precursor synthesis method governs the Li⁺ concentration by varying

LiNH₂ contents and the fact that the as-synthesized polymer precursor is already in THF solution eases the way to disperse with the PEO host. (3) The other is to optimize the intrinsic composition of the polymer to increase Li⁺ diffusion (i.e., increasing the N/P ratio) and decrease anion transport. Figure 5a shows the Nyquist plots of the 60PEO/Li₃PON, Li₆PON, Li₅SiPON, Li₂SiPHN, and Li₆SiPON composite films at ambient.

The in-plane ionic conductivity and activation energies were calculated following the eqs 1 and 2, respectively

$$\sigma = t/(A_e * R) \tag{1}$$

$$\sigma_T = \sigma_o \exp\left(-\frac{E_a}{k_B T}\right) \tag{2}$$

where t is the thickness of the film, $A_{\rm e}$ is the area of the electrode, R is the resistivity acquired from the Nyquist plot, $\sigma_{\rm o}$ is the pre-exponential factor, $E_{\rm a}$ is the activation energy, $k_{\rm B}$ is the Boltzmann constant, and T is the absolute temperature.

Table 4 lists the total room-temperature conductivities of the PE films heated to 65 °C/12 h/Vac. The PEO/Li₃SiPON composite film offers the highest conductivity of 2.8×10^{-3} S/cm. The as-cast and warmed PEO/polymer films offered thicknesses in the range of 25–50 μ m.

Figure 5b demonstrates the relation between the N/P ratio, crystallinity percentage, and ionic conductivity of the polymer electrolytes. Here, we have demonstrated that the ionic conduction mechanism of the PEs depends on both the N/P ratio and the nature of the amorphous phase obtained from XPS (Table 2) and DSC (Table 3) data, respectively. The reported N/P ratios in this study are relatively high compared to the gas-phase-deposited Li_xPON electrolytes, which result in significant improvements in the ionic conductivity. The decrease in electrostatic energy as a result of more $P-N<_p^P$ cross-link structures in the PEs is one of the main factors contributing to the increase in Li⁺ mobility. The structures

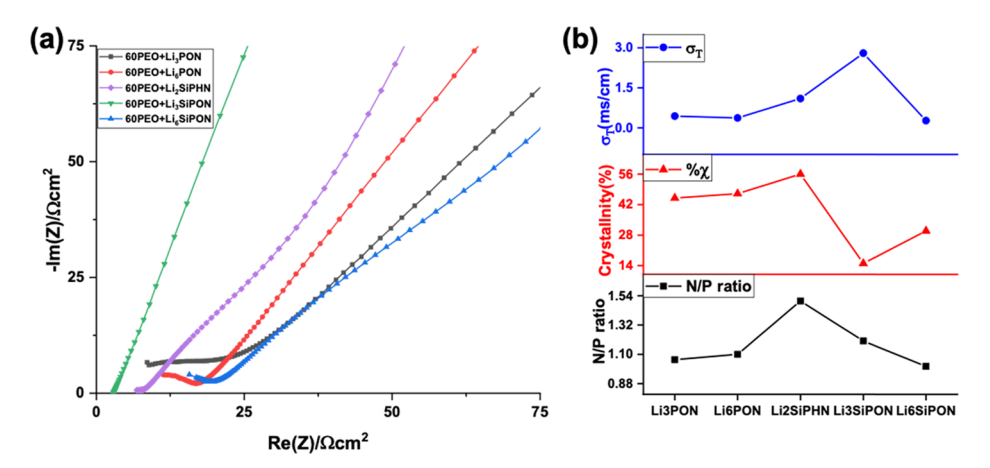


Figure 5. (a) Nyquist plots of PEs at ambient and (b) correlation between the N/P ratio (black), crystallinity percentage (red), and ionic conductivity of PEs (blue).

Table 4. Total Room-Temperature Conductivity of PEs

precursor	conductivity (S/cm)
Li ₃ PON	$4.4 \pm 0.6 \times 10^{-4}$
Li ₆ PON	$3.7 \pm 0.4 \times 10^{-4}$
Li ₂ SiPHN	$1.1 \pm 0.3 \times 10^{-3}$
Li ₃ SiPON	$2.8 \pm 0.2 \times 10^{-3}$
Li ₆ SiPON	$2.7 \pm 0.1 \times 10^{-4}$

of the polymer precursors are shown in Schemes S1 and S2. The 60PEO/Li₂SiPHN showed the highest N/P ratio (1.5), resulting in a decrease in electrostatic energy; however, this alone did not result in fast ion mobility compared to the 60PEO/Li₃SiPON thin film. This is ascribed to the fact that the 60PEO/Li₂SiPHN film showed the highest crystalline percentage (~56%). Similar phenomena are observed for the 60PEO/Li_xPON polymer electrolytes. This indicates that the main limiting factor for fast Li⁺ diffusion is the mobility of the PEO matrix. Although some reports show that crystalline PEO can offer fast ionic transport, prevailingly, the crystalline region of the PEO is a detrimental factor owning to the slower chain dynamics upon crystallization resulting in the decreased ionic conductivity.⁵⁸

The decrease in the crystallinity of $60PEO/Li_3SiPON$ (~15%) along with the high N/P ratio resulted in superior ionic conductivity 2.8×10^{-3} S/cm at ambient in good agreement with DSC (Figure 4), in situ XRD (Figure 1), and XPS data (Figure 2). This value is much higher than gas-phase-deposited Li_xPON typically 10^{-6} S/cm⁵⁹ at ambient and higher than simple PEO/Li⁺ salt polymers.⁵² This is ascribed to the solvation ability of the polymer backbone and homogenous miscibility of the polymer precursor in the PEO, as shown by the optical image of Figure 3a. For comparison, the ionic conductivity of the polymer electrolytes with different Li salts and plasticizers at room temperature is listed in Table S3.

The solvation state of Li⁺ ions highly depends on the polymer backbone, bearing the ionic group. The Li_xSiPON polymer precursor with high nitrogen atoms appears to favor Li solvation compared to the Li_xPON polymer precursors. Charge transport requires both efficient ionic solvation and a low migration barrier. Hence, the solvated Li⁺ ion mobility must be optimized through the polymer matrix to produce superionic polymer electrolyte thin films, which requires the amorphous nature of the PEO matrix.²⁷

A key design factor for the PEO-based electrolytes is generally to suppress the crystallinity and increase the amorphous wt % fraction for ion transport. 12 Generally, lithium salt with bulkier anions is preferred, due to the welldelocalized negative charge promoting fast Li+ diffusion and improving the ionic conductivity. 60 As the predominant ionic diffusion occurs in the amorphous region of PEO, segmental motion and local relaxation of the PEO matrix are needed for Li⁺ transport. The proposed Li⁺ ion conduction mechanism for the PEO/Li salt is through a segmental motion, where the Li⁺ ions are coordinated by the ether oxygen atom. 12 In the PEO/ Li salt systems, both the cations and anions are mobile species, resulting in a decrease in the transference numbers, which is generally < 0.5 due to the electropolarization from anion buildup. 61 The electropolarization can lead to a decrease in the electrochemical performance due to high internal impedance, IR drops, and dendritic growth.⁶²

The single-ion conductor can overcome these challenges faced by salt-doped counterparts. Previous studies indicate that high ionic dissociation and enhancement in the concentration of charge carriers can be achieved by introducing nitrogen atoms into the backbone of the polymer, which is known to decrease the anion-cation binding energies. 61,63 The anions of the polymer precursors (Li_xPON and Li_xSiPON) are proposed to be chemically bound with the PEO polymer backbone, resulting in only cation transport. The anionic units in these polymer precursors/PEO mixtures are predicted to be immobile in regard to conductivity. This theory is supported by the achieved high ionic conductivity at ambient, a very low activation energy, high t_{Li^+} , and the stability of the PEs in symmetric and half-cell configurations discussed below. The difference in solvation might be related to the property of the interface between the PEO-functionalized segments and the polymer precursors.

Lithium transference number was determined following a procedure described elsewhere.³⁸ The stability of PEs against the metallic Li anode was analyzed by observing the Nyquist plots of the Li/60 wt % PEO/PEs/Li symmetrical cells before and after chronoamperometry measurements at ambient. Figure S3a—d shows the Nyquist and chronoamperometry plots of symmetric cells assembled with the 60PEO/Li₃PON and 60PEO/Li₆PON electrolytes. The Nyquist plots (Figure S3c) for the Li₆PON system demonstrate that the resistance is almost constant before and after steady-state current.

Conversely, the Li₃PON polymer electrolyte showed an increase in resistivity after the chronoamperometry measurement (Figure S3b).

The Ohmic region of the cell impedance is usually associated with the high-frequency range semicircle, which is associated with the resistance of the PEs, the semicircle at low frequencies is attributed to the capacitive properties, solid electrolyte interface (SEI). Both the Nyquist plots (Figure S4a) for the 60PEO/Li₃PON system start at the same Ohmic region, and thus, the impedance of this system is the same before and after chronoamperometry measurement. Thus, the increase in resistance at lower frequencies for the 60PEO/Li₃PON system has to be associated with the formation of SEI and charge-transfer resistance at the Li electrodes.

Figure S4a-d shows the Nyquist and chronoamperometry plots of symmetric cells assembled with the $60PEO/Li_2SiPHN$ and $60PEO/Li_6SiPON$ polymer electrolytes. Both Nyquist plots exhibit that the resistance is nearly constant before and after steady-state current. Table 5 lists the $t_{1,i}$ of the various PE

Table 5. Li⁺ Transfer Numbers of PEs

sample	t_{Li^+} avg
Li ₃ PON	0.6 ± 0.05
Li ₆ PON	0.5 ± 0.07
Li ₂ SiPHN	0.8 ± 0.01
Li ₆ SiPON	0.65 ± 0.05

films. The increase in the t_{Li^+} for the PE films suggests that the chemical interaction between Li and PON, SiPON, and SiPHN results in fast Li⁺ mobility.

The Li₂SiPHN precursor showed a high $t_{\rm Li^+}$ of ~0.8 comparable to the single-ion conducting polymer electrolytes. The transference number decreased for the PEO-based PE films compared to pristine Li_xPON polymer precursors. This might be ascribed to the increasing mobility of both cation and anion in the PE film due to high flexibility of the PEO segments. The increase in the transference number of Li₂SiPHN might be due to the cyclometric structure of SiPHN; the molecule is bulkier than SiPON and PON, hence lower anion mobility. One method to obtain the single-ion conducting PE is by anchoring the anions to the polymer backbone. It

Figure S5 shows the typical Arrhenius plots for the PEs films, where AC impedance measurements were performed in a frequency range of 7 MHz to 1 Hz at -15 to 70 °C. The activation energy is the sum of the energy required to form defects and the ion migration energy, which was obtained by linear fitting of the log conductivity with 1/T plots. The linear fit of the Arrhenius plots was used to calculate the activation energies of the PEs, as listed in Table S4. The decrease in activation energies in the PEs is ascribed to the

increase in mobile Li⁺-ion concentration and the decrease in PEO crystallinity.

Table 6 records the total ionic conductivities of the PE films heated to selected temperatures. Optimization of ionic conductivity was achieved by introducing the ionically conducting PEs, which are key to improving the room temperature and reducing the activation energy for cation transport.

The temperature-dependent conductivity of the PEs increases with increases in temperature for all PEO/precursor systems. The activation energies decrease from 0.5 to 0.23 eV for the Li₂SiPHN νs Li₃PON precursor. This latter value is ascribed to the amorphous nature of the PE, hindering the crystallinity of the PEO and facilitating fast Li⁺ motion as supported by DSC data.

3.2. Symmetric Studies of Li/PEs/Li. Figure 6a–c shows the galvanostatic cycling of Li/60PEO/Li₃PON, Li₂SiPHN, and Li₆SiPON/Li at ambient. The symmetric cells show nearly constant voltage responses of 3, 2, and 30 mV for Li₃PON-, Li₂SiPHN-, and Li₆SiPON-based PEs, respectively. These results suggest that the PEs are stable *vs* Li metal at higher current densities (0.325 mA/cm²) compared to the conventional PEO/Li salt electrolytes (0.1 mA/cm²).^{64,65}

Figure 6d shows the galvanostatic cycling of Li/60PEO/Li₆PON/Li at room temperature. The main goal of the symmetric cell experiment was to increase the current densities and study the interfacial behavior of the electrode—electrolyte such that an optimal c-rate is used when the half-cell is assembled.

The symmetric cell shows a stable voltage response of 0.02 V for the first 40 h; the interfacial resistance seems to increase as demonstrated by the increase in voltage to 0.05 V after the 20th cycle. The 60PEO/Li₆PON film is stable *vs* Li metal at higher current densities (3.25 mAh/cm²) compared to the traditional PEO/Li salt electrolytes (0.1 mA/cm²).⁶⁴ It is also worth mentioning that these symmetric cell studies are performed at room temperature, while most PEO/Li salt studies are performed at elevated temperatures (>65 °C).⁶⁵ Most polymer/solid electrolytes are limited by the solid—solid diffusion at the interface, resulting in a reduction of the critical current densities.⁶⁶ Here, we are able to enhance the interface between the Li metal electrode and the polymer films by melt bonding the PEs on top of the Li surface.

The development of high energy density ASSBs depends on the stability of the solid electrolyte at wide potentials. CV was carried out at a scanning rate of 5 mV/s at ambient to examine the electrochemical stability of the PE films. Figure S6 shows CVs acquired for the Li/PEs/SS cell in the ranges of -1 to 6 V. The cathodic and anodic peaks \sim 0 V suggest lithium plating and stripping, demonstrating that Li⁺ ions can migrate through PEs and deposit on the stainless steel side and vice versa. At

Table 6. Total Conductivities (σ_t) of PEs Heated to Selected Temperatures

T (°C)	σ (S/cm) Li ₃ PON	σ (S/cm) Li ₆ PON	σ (S/cm) Li ₂ SiPHN	σ (S/cm) Li ₃ SiPON	σ (S/cm) Li ₆ SiPON
-15	1.4×10^{-4}	1.9×10^{-5}	4.6×10^{-5}	4.2×10^{-5}	4×10^{-5}
0	2.8×10^{-4}	6.3×10^{-4}	1×10^{-4}	5.2×10^{-5}	5×10^{-5}
25	4.7×10^{-4}	9.4×10^{-4}	1.6×10^{-3}	2.8×10^{-4}	2.7×10^{-4}
35	7×10^{-4}	1.7×10^{-3}	3.5×10^{-3}	3.5×10^{-4}	5.4×10^{-4}
45	1.1×10^{-3}	1.9×10^{-3}	4.4×10^{-3}	4.7×10^{-4}	5.6×10^{-4}
65	1.2×10^{-3}	4.7×10^{-3}	1.3×10^{-2}	1×10^{-3}	1.6×10^{-3}
70	1.9×10^{-3}	$7. \times 10^{-3}$	1.8×10^{-2}	1.2×10^{-3}	1.7×10^{-3}

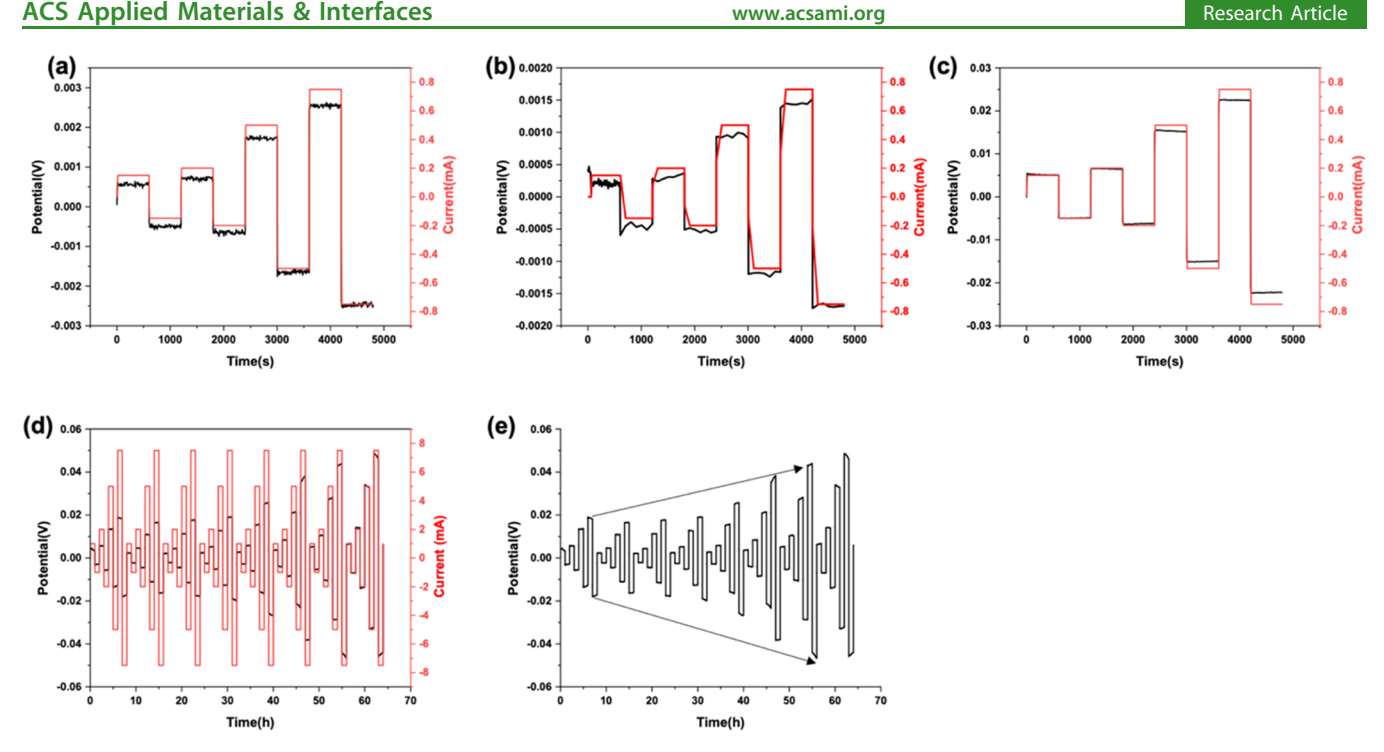


Figure 6. Galvanostatic cycling of Li/60PEO: (a) Li₃PON, (b) Li₂SiPHN, (c) Li₆SiPON/Li symmetric cells at the current density of $\pm 0.15-0.75$ mA and (d) Li/60PEO/Li₆PON/Li symmetric cells at the current density of ±1.5-7.5 mA at room temperature. (e) Potential vs time profile of the Li/60PEO/Li₆PON/Li cell.

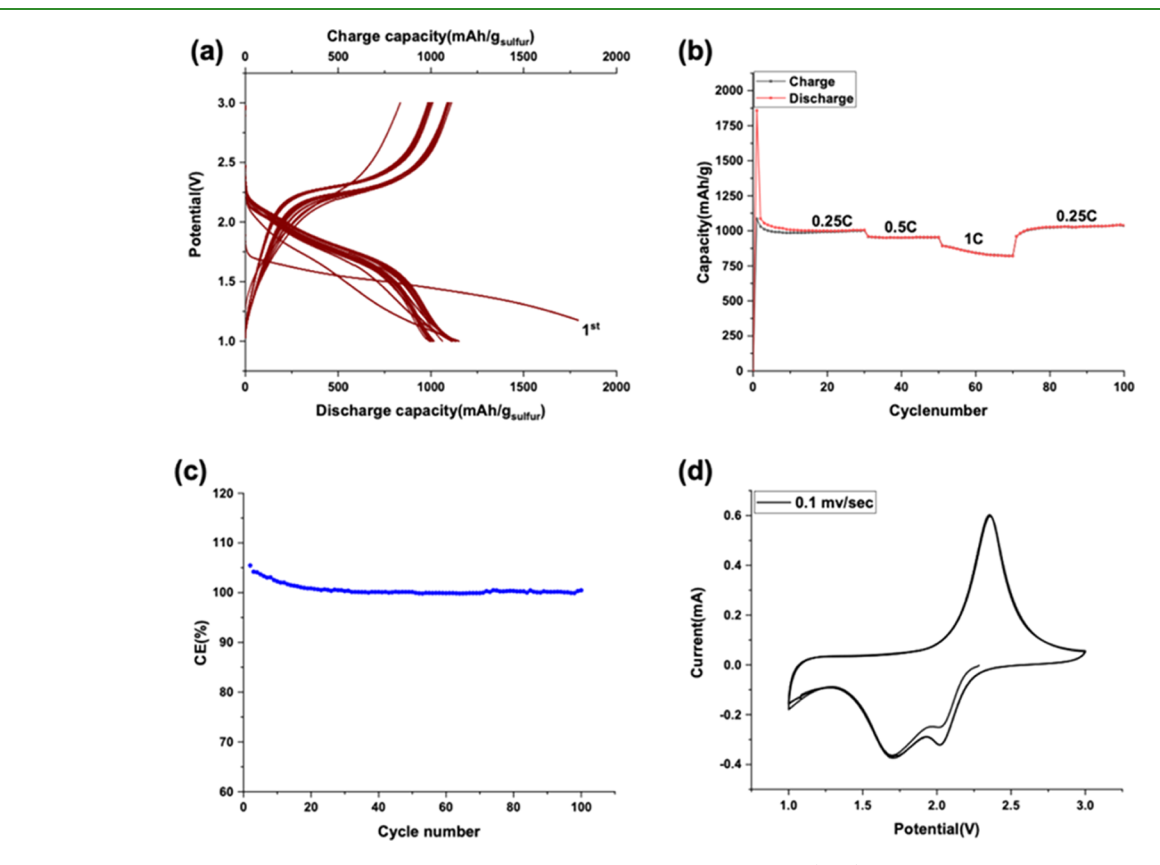


Figure 7. Galvanostatic cycling plots of SPAN/60PEO/Li₆SiPON/Li at selected c-rates (a-c) and cyclic voltammogram at 0.1 mV/s (d).

higher voltage, the current response is quite small, revealing that the PE films offer wide electrochemical stabilities.

3.3. Half-Cell Studies of SPAN/PEs/Li. The composite cathode shows a 3-D network of structures forming microglobules. The EDX map in Figure S7 shows the signature element (S, C, and Al) distribution for SPAN. Figures S8 and S9 show the SEM and EDX images of the SPAN-based active material warm-pressed with 60PEO/Li₃PON and 60PEO/ Li₆PON films, respectively. There is a noticeable interface between the polymer electrolyte, cathode, and current collector. Elemental mapping of the catholyte shows well-defined phosphorus, aluminum, and sulfur interface distributions. The compiled EDX image also shows a clear elemental layered structure where C, N, and P are in the top region ascribed to the polymer electrolyte, the middle region is mostly occupied by sulfur, and the bottom is dominated by Al.

Figures S10 and S11 show the SEM and EDX images of SPAN/60PEO/Li₂SiPHN and 60PEO/Li₆SiPON warm-pressed at 5 kpsi/40 °C/2 min, respectively. The SPAN cathode warm-pressed with 60PEO/Li₂SiPHN and 60PEO/Li₆SiPON films present very smooth and uniform interfaces, ideal catholytes. The EDX map shows well-distributed elements (Si, P, and O) at the top of the image ascribed to the polymer precursors, C is also dominant in the middle region along with S, attributed to the cathode. The bottom interface is mainly composed of Al from the current collector.

Figures S12 and S13 show the Nyquist plot for the SPAN/PEs/Li half-cell at ambient before cycling. The resulting equivalent series resistance and open circuit potentials are listed in Table S5. EIS measurements were carried out to analyze the impedance disparities of the half-cells when using the various PE films. All of the Nyquist plots have a tail at lower-frequency regions ascribed to the Warburg impedance of Li⁺ diffusion in the electrodes.

Figure 7a illustrates the result of the SPAN/60PEO/ Li₆SiPON/Li cells cycled at various C rates. The Li-SPAN battery cycled for 500 h with minimal voltage fluctuation. The half-cell was cycled from 1 to 3 V for 100 cycles. The galvanostatic cycling profile shows that the Li-S cell was cycled for 30 cycles at 0.25C, 20 cycles at 0.5 and 1C, and the last 20 cycles at 0.25C. During the initial discharge cycle, the obtained voltage plateau (~1.5 V) is lower than the potentials observed in succeeding cycles, as shown in Figure 7a. This suggests that the discharge process involves a different reaction. In the subsequent cycles, the voltage profile shows an increase in the discharge plateau (1.7 V). The obtained voltage plateaus are obviously different from what is commonly reported for the Li-S cells, where a two-step voltage plateau is reported ascribed to the reaction of Li⁺ and elemental sulfur to form lithium polysulfides ~2.4 V. The second plateau ~2.1 V is associated with the formation of short-order polysulfide. 53,67,68 The presence of only one voltage plateau $\sim 2.2~V$ is vital as it suggests that lithium polysulfides do not form in the Li-SPAN cell, which suppresses the polysulfide shuttle effect and maximizes cycle life, this is typical for the SPAN cathodes. 69 The plausibility of this hypothesis is also supported by the high coulombic efficiency.

The half-cell showed initial discharge capacities of \sim 1800 mAh/g_{sulfur}, higher than the theoretical capacity for sulfur (1672 mAh/g), as seen in Figure 7a. This suggests that the carbon framework of SPAN (π -conjugated pyridinic) contributes to the initial capacity. It is probably a mixture of Faradic capacity as a result of SEI formation on carbon during the initial cycle and a non-Faradic pseudocapacitance. ^{68,69}

The half-cell charges and discharges to the targeted potentials with minimal polarization for 100 cycles at the desired C-rates. The capacity starts to decrease to 1000 mAh/ g_{sulfur} after the first cycle. The capacity showed a slight decrease to 950 and 800 mAh/ g_{sulfur} at 0.5 and 1C; however, the capacity was recovered when cycled back to 0.25C. The Li/S cathode shows high capacity, high cycle stability, and high discharge/charge capacity. The 60PEO/Li₆SiPON polymer electrolyte also showed high electrochemical stability at high

rates of 0.25, 0.5, and 0.1C for 100 cycles. A coulombic efficiency of \sim 100% was maintained throughout the cycle.

Figure 7d shows the cyclic voltammogram of SPAN/60PEO/Li₆SiPON/Li. CV provides additional information about the electrochemical property of the SPAN cathode and the PE film. It is possible to confirm that sulfur as S_2 and S_3 are the major species in the SPAN electrode. ^{69,70} The CV curves show multiple redox peaks; note that the lower voltage plateau for the initial discharge process is in a good agreement with the voltage profile obtained from the galvanostatic cycling studies shown in Figure 7a.

If these PEO/polymer precursors can be melt cast onto the cathodes and Li metal at the melting point of PEO $(65-75\,^{\circ}\text{C})$, it may be possible to replace the liquid electrolytes in traditional Li-ion batteries with melt cast mixtures of these materials eliminating fire hazards, reducing the extent of containment seals needed, and perhaps greatly simplifying the ASSB assembly.

4. CONCLUSIONS

We describe here a comparative evaluation of different types of polymer precursors (Li_xPON, Li_xSiPHN, and Li_xSiPON) on the PEO-derived composite films. These active fillers were synthesized via a novel polymer precursor route with controlled lithiation, resulting in a remarkable enhancement on the cation transport. The increase in Li⁺ ion concentration and the addition of secondary phase (PON) resulted in a decrease in activation energy for the PEO/Li_xPON films, indicating a high dissociation ability to yield mobile cations.

A maximum ionic conductivity of 2.8×10^{-3} S/cm is achieved for the 60PEO/Li₃SiPON films at ambient. The enhancement in conductivity of this PE is ascribed to the suppression of the PEO crystallinity and the increase in the N/P ratio. The Li_xSiPON polymer precursor with high nitrogen atoms seems to favor lithium solvation better than the Li_xPON polymer precursors. Besides, the high Li⁺ transference number of Li₂SiPHN indicates that the mobility of anions has been limited ascribed to the polymer precursor backbone. In addition to the enhanced ionic conductivities vs traditional PEO electrolytes, these active polymer precursor fillers offer improved stability against lithium metal at higher current densities. Galvanostatic cycling of the SPAN/PEs/Li cell shows discharge capacities of 1000 mAh/g_{sulfur} at 0.25C and 800 mAh/g_{sulfur} at 1C. The cell also shows high capacity retention over 100 cycles with 100% coulombic efficiencies.

ASSOCIATED CONTENT

Supporting Information

The Supporting Information is available free of charge at https://pubs.acs.org/doi/10.1021/acsami.0c06196.

The analytical tools and the microstructure images of the cathode/polymer electrolyte interfaces are provided (PDF)

AUTHOR INFORMATION

Corresponding Author

Richard M. Laine — Department of Materials Science and Engineering, University of Michigan, Ann Arbor, Michigan 48109-2136, United States; orcid.org/0000-0003-4939-3514; Phone: +1 734 764-6203; Email: talsdad@umich.edu

Authors

Eleni Temeche – Department of Materials Science and Engineering, University of Michigan, Ann Arbor, Michigan 48109-2136, United States

Xinyu Zhang — Department of Materials Science and Engineering, University of Michigan, Ann Arbor, Michigan 48109-2136, United States

Complete contact information is available at: https://pubs.acs.org/10.1021/acsami.0c06196

Author Contributions

All authors have given approval to the final version of the manuscript.

Funding

DOE through Batt500 Seedling project DE-EE0008235, Mercedes-Benz Research & Development North America (MBRDNA), and DMR NSF Grant No. DMR 099217.

Notes

The authors declare no competing financial interest.

ACKNOWLEDGMENTS

This work was supported by DOE through the Batt500 Seedling project DE-EE0008235 and a gift from Mercedes-Benz Research & Development North America (MBRDNA). A portion of this work was also supported by a DMR NSF Grant No. DMR 099217. We especially thank Tobias Glossman for his encouragement.

DEDICATION

Dedicated to the memory of Prof. Dr. Andreas Hintennach, friend and mentor deceased May 10, 2020.

■ REFERENCES

- (1) Xu, W.; Wang, J.; Ding, F.; Chen, X.; Nasybulin, E.; Zhang, Y.; Zhang, J. G. Lithium Metal Anodes for Rechargeable Batteries. *Energy Environ. Sci.* **2014**, *7*, 513–537.
- (2) Manthiram, A.; Yu, X.; Wang, S. Lithium Battery Chemistries Enabled by Solid-State Electrolytes. *Nat. Rev. Mater.* **2017**, 2, No. 16103.
- (3) Kalhoff, J.; Eshetu, G. G.; Bresser, D.; Passerini, S. Safer Electrolytes for Lithium-Ion Batteries: State of the Art and Perspectives. *ChemSusChem* **2015**, *8*, 2154–2175.
- (4) Fergus, J. W. Ceramic and Polymeric Solid Electrolytes for Lithium-Ion Batteries. *J. Power Sources* **2010**, *195*, 4554–4569.
- (5) Yi, E.; Wang, W.; Mohanty, S.; Kieffer, J.; Tamaki, R.; Laine, R. M. Materials That Can Replace Liquid Electrolytes in Li Batteries: Superionic Conductivities in Li1.7Al0.3Ti1.7Si 0.4P2.6O12. Processing Combustion Synthesized Nanopowders to Free Standing Thin Films. *J. Power Sources* **2014**, *269*, 577–588.
- (6) Yi, E.; Wang, W.; Kieffer, J.; Laine, R. M. Flame Made Nanoparticles Permit Processing of Dense, Flexible, Li⁺ Conducting Ceramic Electrolyte Thin Films of Cubic-Li₇La₃Zr₂O₁₂ (c-LLZO). *J. Mater. Chem. A* **2016**, *4*, 12947–12954.
- (7) Masoud, E. M.; El-Bellihi, A. A.; Bayoumy, W. A.; Mousa, M. A. Effect of LiAlO2 Nanoparticle Filler Concentration on the Electrical Properties of PEO-LiClO4 Composite. *Mater. Res. Bull.* **2013**, *48*, 1148–1154.
- (8) Manuel Stephan, A.; Nahm, K. S. Review on Composite Polymer Electrolytes for Lithium Batteries. *Polymer* **2006**, *47*, 5952–5964.
- (9) Fenton, D. E.; Parker, J. M.; Wright, P. V. Complexes of Alkali Metal Ions with Poly(Ethylene Oxide). *Polymer* 1973, 14, No. 589.
- (10) Angulakshmi, N.; Nahm, K. S.; Swaminathan, V.; Thomas, S.; Nimma Elizabeth, R. Nanocomposite Polymer Electrolytes for Lithium Batteries. *Polym. Process. Charact.* **2012**, DOI: 10.1201/b13105.

- (11) Long, L.; Wang, S.; Xiao, M.; Meng, Y. Polymer Electrolytes for Lithium Polymer Batteries. *J. Mater. Chem. A* **2016**, *4*, 10038–10069.
- (12) Borodin, O.; Smith, G. D. Mechanism of Ion Transport in Amorphous Poly(Ethylene Oxide)/LiTFSI from Molecular Dynamics Simulations. *Macromolecules* **2006**, *39*, 1620–1629.
- (13) Scrosati, B.; Croce, F.; Persi, L.; Persi, L. Impedance Spectroscopy Study of PEO-Based Nanocomposite Polymer Electrolytes. *J. Electrochem. Soc.* **2002**, *147*, No. 1718.
- (14) Berthier, C.; Gorecki, W.; Minier, M.; Armand, M. B.; Chabagno, J. M.; Rigaud, P. Microscopic Investigation of Ionic Conductivity in Alkali Metal Salts-Poly(Ethylene Oxide) Adducts. *Solid State Ionics* 1983, 11, 91–95.
- (15) Cameron, G. G.Solid Polymer Electrolytes: Fundamentals and Technological Applications. Fiona, M. Gray.. VCH Publishers Inc.: New York 1991. Pp. x + 245, Price £44.00. ISBN 0-89573-772-8. *Polym. Int.*2007. https://doi.org/10.1002/pi.4990320421.
- (16) Stoeva, Z.; Martin-Litas, I.; Staunton, E.; Andreev, Y. G.; Bruce, P. G. Ionic Conductivity in the Crystalline Polymer Electrolytes PEO6:LiXF6, X = P, As, Sb. J. Am. Chem. Soc. 2003, 125, 4619–4626.
- (17) Sun, J.; Liao, X.; Minor, A. M.; Balsara, N. P.; Zuckermann, R. N. Morphology-Conductivity Relationship in Crystalline and Amorphous Sequence-Defined Peptoid Block Copolymer Electrolytes. *J. Am. Chem. Soc.* **2014**, *136*, 14990–14997.
- (18) MacGlashan, G. S.; Andreev, Y. G.; Bruce, P. G. Structure of the Polymer Electrolyte Poly (Ethylene Oxide) 6: LiAsF6. *Nature* **1999**, 398, 792–794.
- (19) Gadjourova, Z.; Andreev, Y. G.; Tunstall, D. P.; Bruce, P. G. Ionic Conductivity in Crystalline Polymer Electrolytes. *Nature* **2001**, 412, 520–523.
- (20) Christie, A. M.; Lilley, S. J.; Staunton, E.; Andreev, Y. G.; Bruce, P. G. Increasing the Conductivity of Crystalline Polymer Electrolytes. *Nature* **2005**, 433, 50–53.
- (21) Liu, W.; Liu, N.; Sun, J.; Hsu, P. C.; Li, Y.; Lee, H. W.; Cui, Y. Ionic Conductivity Enhancement of Polymer Electrolytes with Ceramic Nanowire Fillers. *Nano Lett.* **2015**, *15*, 2740–2745.
- (22) Michael, M.; Jacob, M. M.; Prabaharan, S. R.; Radhakrishna, S. Enhanced Lithium Ion Transport in PEO-Based Solid Polymer Electrolytes Employing a Novel Class of Plasticizers. *Solid State Ionics* **2002**, *98*, 167–174.
- (23) Kumar, Y.; Hashmi, S. A.; Pandey, G. P. Lithium Ion Transport and Ion-Polymer Interaction in PEO Based Polymer Electrolyte Plasticized with Ionic Liquid. *Solid State Ionics* **2011**, *201*, 73–80.
- (24) El Bellihi, A. A.; Bayoumy, W. A.; Masoud, E. M.; Mousa, M. A. Preparation, Characterizations and Conductivity of Composite Polymer Electrolytes Based on PEO-LiClO 4 and Nano ZnO Filler. *Bull. Korean Chem. Soc.* **2012**, *33*, 2949–2954.
- (25) Gao, S.; Yan, X. L.; Zhong, J.; Xue, G. B.; Wang, B. Temperature Dependence of Conductivity Enhancement Induced by Nanoceramic Fillers in Polymer Electrolytes. *Appl. Phys. Lett.* **2013**, *102*, No. 173903.
- (26) Wang, G. X.; Yang, L.; Wang, J. Z.; Liu, H. K.; Dou, S. X. Enhancement of Ionic Conductivity of PEO Based Polymer Electrolyte by the Addition of Nanosize Ceramic Powders. *J. Nanosci. Nanotechnol.* **2005**, *S*, 1135–1140.
- (27) Wang, Y.-J.; Pan, Y.; Chen, L. Ion-Conducting Polymer Electrolyte Based on Poly(Ethylene Oxide) Complexed with Li1.3Al0.3Ti1.7(PO4)3 Salt. *Mater. Chem. Phys.* **2005**, *92*, 354–360.
- (28) Wang, W.; Yi, E.; Fici, A. J.; Laine, R. M.; Kieffer, J. Lithium Ion Conducting Poly(Ethylene Oxide)-Based Solid Electrolytes Containing Active or Passive Ceramic Nanoparticles. *J. Phys. Chem. C* **2017**, 121, 2563–2573.
- (29) Zhao, E.; Ma, F.; Guo, Y.; Jin, Y. Stable LATP/LAGP Double-Layer Solid Electrolyte Prepared: Via a Simple Dry-Pressing Method for Solid State Lithium Ion Batteries. *RSC Adv.* **2016**, *6*, 92579–92585.
- (30) Bates, J. B.; Dudney, N. J.; Gruzalski, G. R.; Zuhr, R. A.; Choudhury, A.; Luck, C. F.; Robertson, J. D. Fabrication and Characterization of Amorphous Lithium Electrolyte Thin Films and

- Rechargeable Thin-Film Batteries. J. Power Sources 1993, 43, 103-110.
- (31) Yu, X. A Stable Thin-Film Lithium Electrolyte: Lithium Phosphorus Oxynitride. J. Electrochem. Soc. 1997, 144, No. 524.
- (32) Wang, C.; Bai, G.; Yang, Y.; Liu, X.; Shao, H. Dendrite-Free All-Solid-State Lithium Batteries with Lithium Phosphorous Oxynitride-Modified Lithium Metal Anode and Composite Solid Electrolytes. *Nano Res.* **2019**, *12*, 217–223.
- (33) Liu, W.-Y.; Fu, Z.-W.; Li, C.-L.; Qin, Q.-Z. Lithium Phosphorus Oxynitride Thin Film Fabricated by a Nitrogen Plasma-Assisted Deposition of E-Beam Reaction Evaporation. *Electrochem. Solid-State Lett.* **2004**, *7*, No. J36.
- (34) Dudney, N. J. Thin Film Micro-Batteries. *Electrochem. Soc. Interface* **2008**, *17*, 44.
- (35) Zhang, T.; Imanishi, N.; Hasegawa, S.; Hirano, A.; Xie, J.; Takeda, Y.; Yamamoto, O.; Sammes, N. Li/Polymer Electrolyte/Water Stable Lithium-Conducting Glass Ceramics Composite for Lithium-Air Secondary Batteries with an Aqueous Electrolyte. *J. Electrochem. Soc.* 2008, 155, No. A965.
- (36) Kumar, B.; Kumar, J.; Leese, R.; Fellner, J. P.; Rodrigues, S. J.; Abraham, K. M. A Solid-State, Rechargeable, Long Cycle Life Lithium—Air Battery. *J. Electrochem. Soc.* **2010**, *157*, No. A50.
- (37) Jadhav, H. S.; Kalubarme, R. S.; Jadhav, A. H.; Seo, J. G. Highly Stable Bilayer of LiPON and B2O3 Added Li1.5Al0.5Ge1.5(PO4) Solid Electrolytes for Non-Aqueous Rechargeable Li-O2 Batteries. *Electrochim. Acta* **2016**, DOI: 10.1016/j.electacta.2016.03.143.
- (38) Temeche, E.; Zhang, X.; Laine, R. M. Polymer Precursor Derived Li x PON Electrolytes: Toward Li S Batteries. ACS Appl. Mater. Interfaces 2020, 12, 20548–20562.
- (39) Zhang, X.; Temeche, E.; Laine, R. M. Design, Synthesis, and Characterization of Polymer Precursors to LixPON and LixSiPON Glasses: Materials That Enable All-Solid-State. *Macromolecules* **2020**, 53, 2702–2712.
- (40) Temeche, E.; Yi, E.; Keshishian, V.; Kieffer, J.; Laine, R. M. Liquid-Feed Flame Spray Pyrolysis Derived Nanopowders (NPs) as a Route to Electrically Conducting Calcium Aluminate (12CaO.7A-12O3) Films. J. Eur. Ceram. Soc. 2019, 39, 1263–1270.
- (41) Zhao, Y.; Zhang, Y.; Gosselink, D.; Doan, T. N. L.; Sadhu, M.; Cheang, H. J.; Chen, P. Polymer Electrolytes for Lithium/Sulfur Batteries. *Membranes* **2012**, *2*, 553–564.
- (42) Bannister, D. J.; Davies, G. R.; Ward, I. M.; McIntyre, J. E. Ionic Conductivities for Poly(Ethylene Oxide) Complexes with Lithium Salts of Monobasic and Dibasic Acids and Blends of Poly(Ethylene Oxide) with Lithium Salts of Anionic Polymers. *Polymer* 1984, 25, 1291–1296.
- (43) Laine, R. M. Transformation of Organometallics into Common and Exotic Materials: Design and Activation; Springer, 1988.
- (44) Laine, R. M.; Sellinger, A. Si-Containing Ceramic Precursors. *The Chemistry of Organic Silicon Compounds* **2003**, 2245–2316.
- (45) Okamura, K. Ceramic Fibres from Polymer Precursors. *Composites* **1987**, *18*, 107–120.
- (46) Greil, P. Polymer Derived Engineering Ceramics. Adv. Eng. Mater. 2000, 2, 339–348.
- (47) Lee, S.-J.; Bae, J. H.; Lee, H. W.; Baik, H. K.; Lee, S. M. Electrical Conductivity in Li-Si-P-O-N Oxynitride Thin-Films. *J. Power Sources* **2003**, *123*, 61–64.
- (48) Lee, S.-J.; Baik, H.-K.; Lee, S.-M. An All-Solid-State Thin Film Battery Using LISIPON Electrolyte and Si-V Negative Electrode Films. *Electrochem. Commun.* **2003**, *5*, 32–35.
- (49) Su, Y.; Falgenhauer, J.; Leichtweiß, T.; Geiß, M.; Lupó, C.; Polity, A.; Zhou, S.; Obel, J.; Schlettwein, D.; Janek, J.; Meyer, B. K. Electrochemical Properties and Optical Transmission of High Li+Conducting LiSiPON Electrolyte Films. *Phys. Status Solidi* **2017**, 254, No. 1600088.
- (50) Laine, R. M.; Kim, S. G.; Rush, J.; Tamaki, R.; Wong, E.; Mollan, M.; Sun, H. J.; Lodaya, M. Ring-Opening Polymerization of Epoxy End-Terminated Polyethylene Oxide (PEO) as a Route to Cross-Linked Materials with Exceptional Swelling Behavior. *Macromolecules* **2004**, *37*, 4525–4532.

- (51) Kim, Y. G.; Wadley, H. N. G. Lithium Phosphorous Oxynitride Films Synthesized by a Plasma-Assisted Directed Vapor Deposition Approach. J. Vac. Sci. Technol. A Vacuum, Surfaces, Film 2008, 26, 174–183
- (52) Gurusiddappa, J.; Madhuri, W.; Padma Suvarna, R.; Priya Dasan, K. Studies on the Morphology and Conductivity of PEO/LiClO4. *Mater. Today: Proc.* **2016**, 3, 1451–1459.
- (53) Geschke, D. Physical Properties of Polymers Handbook. Zeitschrift für Phys. Chemie 1997, 199, 128.
- (54) Afifi-Effat, A. M.; Hay, J. N. Enthalpy and Entropy of Fusion and the Equilibrium Melting Point of Polyethylene Oxide. *J. Chem. Soc. Faraday Trans.* 2 *Mol. Chem. Phys.* **1972**, DOI: 10.1039/f29726800656.
- (55) Roh, N. S.; Lee, S. D.; Kwon, H. S. Effects of Deposition Condition on the Ionic Conductivity and Structure of Amorphous Lithium Phosphorus Oxynitrate Thin Film. *Scr. Mater.* **1999**, 42, 43–49.
- (56) Morita, M.; Fujisaki, T.; Yoshimoto, N.; Ishikawa, M. Ionic Conductance Behavior of Polymeric Composite Solid Electrolytes Containing Lithium Aluminate. *Electrochim. Acta* **2001**, *46*, 1565–1569.
- (57) Hu, Z.; Li, D.; Xie, K. Influence of Radio Frequency Power on Structure and Ionic Conductivity of LiPON Thin Films. *Bull. Mater. Sci.* **2008**, *31*, 681–686.
- (58) Meabe, L.; Huynh, T. V.; Lago, N.; Sardon, H.; Li, C.; O'Dell, L. A.; Armand, M.; Forsyth, M.; Mecerreyes, D. Poly(Ethylene Oxide Carbonates) Solid Polymer Electrolytes for Lithium Batteries. *Electrochim. Acta* **2018**, *264*, 367–375.
- (59) Pichonat, T.; Lethien, C.; Tiercelin, N.; Godey, S.; Pichonat, E.; Roussel, P.; Colmont, M.; Rolland, P. A. Further Studies on the Lithium Phosphorus Oxynitride Solid Electrolyte. *Mater. Chem. Phys.* **2010**, *123*, 231–235.
- (60) Long, L.; Wang, S.; Xiao, M.; Meng, Y. Polymer Electrolytes for Lithium Polymer Batteries. *J. Mater. Chem. A* **2016**, *4*, 10038–10069.
- (61) Doyle, R. P.; Chen, X.; Macrae, M.; Srungavarapu, A.; Smith, L. J.; Gopinadhan, M.; Osuji, C. O.; Granados-Focil, S. Poly-(Ethylenimine)-Based Polymer Blends as Single-Ion Lithium Conductors. *Macromolecules* **2014**, *47*, 3401–3408.
- (62) Feng, S.; Shi, D.; Liu, F.; Zheng, L.; Nie, J.; Feng, W.; Huang, X.; Armand, M.; Zhou, Z. Single Lithium-Ion Conducting Polymer Electrolytes Based on Poly[(4-Styrenesulfonyl)-(Trifluoromethanesulfonyl)Imide] Anions. *Electrochim. Acta* 2013, 93, 254–263.
- (63) Pehlivan, I. B.; Marsal, R.; Georén, P.; Granqvist, C. G.; Niklasson, G. A. Ionic Relaxation in Polyethyleneimine-Lithium Bis(Trifluoromethylsulfonyl) Imide Polymer Electrolytes. *J. Appl. Phys.* **2010**, *108*, No. 074102.
- (64) Appetecchi, G. B.; Passerini, S. PEO-Carbon Composite Lithium Polymer Electrolyte. *Electrochim. Acta* **2000**, *45*, 2139–2145.
- (65) Bouchet, R.; Lascaud, S.; Rosso, M. An EIS Study of the Anode Li/PEO-LiTFSI of a Li Polymer Battery. *J. Electrochem. Soc.* **2003**, 150, No. A1385.
- (66) Han, X.; Gong, Y.; Fu, K.; He, X.; Hitz, G. T.; Dai, J.; Pearse, A.; Liu, B.; Wang, H.; Rubloff, G.; Mo, Y.; Thangadurai, V.; Wachsman, E. D.; Hu, L. Negating Interfacial Impedance in Garnet-Based Solid-State Li Metal Batteries. *Nat. Mater.* **2017**, *16*, 572–579.
- (67) Mikhaylik, Y. V.; Akridge, J. R. Polysulfide Shuttle Study in the Li/S Battery System. *J. Electrochem. Soc.* **2004**, *151*, No. A1969.
- (68) Cuisinier, M.; Hart, C.; Balasubramanian, M.; Garsuch, A.; Nazar, L. F. Radical or Not Radical: Revisiting Lithium-Sulfur Electrochemistry in Nonaqueous Electrolytes. *Adv. Energy Mater.* **2015**, 5, No. 1401801.
- (69) Wei, S.; Ma, L.; Hendrickson, K. E.; Tu, Z.; Archer, L. A. Metal-Sulfur Battery Cathodes Based on PAN-Sulfur Composites. *J. Am. Chem. Soc.* **2015**, *137*, 12143–12152.
- (70) Frey, M.; Zenn, R. K.; Warneke, S.; Müller, K.; Hintennach, A.; Dinnebier, R. E.; Buchmeiser, M. R. Easily Accessible, Textile Fiber-Based Sulfurized Poly(Acrylonitrile) as Li/S Cathode Material:

Correlating Electrochemical Performance with Morphology and Structure. ACS Energy Lett. 2017, 2, 595–604.

■ NOTE ADDED AFTER ASAP PUBLICATION

This paper was published ASAP on June 22, 2020. Due to production error, many of the authors' corrections were not incorporated. The corrected version was reposted on June 23, 2020.